NeuroImage 99 (2014) 377–387

Contents lists available at ScienceDirect

NeuroImage

journal homepage: www.elsevier.com/locate/ynimg

The effect of linear mixing in the EEG on Hurst exponent estimation

Duncan A.J. Blythe [a,b,*], Stefan Haufe [b,e], Klaus-Robert Müller [b,d], Vadim V. Nikulin [a,c,f]

[a] Bernstein Centre for Computational Neuroscience, Berlin, Germany
[b] Machine Learning Group, Technical University of Berlin, Germany
[c] Neurophysics Group, Charité Medical University, Berlin, Germany
[d] Department of Brain and Cognitive Engineering, Korea University, Seoul, South Korea
[e] Neural Engineering Group, The City College of New York, NY City, USA
[f] Centre for Cognition and Decision Making, National Research University, Higher School of Economics, Moscow, Russia

ARTICLE INFO

Article history:
Accepted 14 May 2014
Available online 24 May 2014

ABSTRACT

Although the long-range temporal correlation (LRTC) of the amplitude fluctuations of neuronal EEG/MEG oscillations is widely acknowledged, the majority of studies to date have been performed in sensor space, disregarding the mixing effects implied by volume conduction and confounding noise. While the effect of mixing on the evaluation of evoked responses and connectivity measures has been extensively studied, there are, to date, no studies reporting on the differences in the values of the estimated Hurst exponents when moving between sensor and source space representations of the multivariate data or on the effect of noise. Such differences, if not duly acknowledged, may lead to erroneous data interpretations. We show in simulations and in theory that measuring Hurst exponents in sensor space may lead to an incomplete picture of the LRTC properties of the underlying data and that noise may significantly bias the estimate of the Hurst exponent of the underlying signal. Moreover, these predictions are confirmed in real data, where we analyze the amplitude dynamics of neuronal oscillations in the resting state from EEG data. By moving either to an independent components representation or to a source representation which maximizes the signal to noise ratio in the alpha frequency range, we observe greater variance, skewness and kurtosis over measured Hurst exponents than in sensor space. We confirm the suitability of conventional source separation methodology by introducing a novel algorithm *HeMax* which obtains a source maximizing the Hurst exponent in the amplitude dynamics of narrow band oscillations. Our findings imply that the long-range correlative properties of the EEG should be studied in source space, in such a way that the SNR is maximized, or at least with spatial decomposition techniques approximating source activities, rather than in sensor space.

Introduction

A widely observed phenomenon in the study of cortical neuronal dynamics is the presence of long-range temporal correlation (LRTC) which corresponds to slowly attenuating autocorrelations or the 1/f shape of the power-spectrum. In EEG and MEG analysis, LRTC time-series include not only the raw electrode data (Miller et al., 2009; Novikov et al., 1997; Pritchard, 1992; Watters and Martin, 2004) but also the amplitude envelopes of narrow band oscillatory signals (Linkenkaer-Hansen et al., 2001; Nikulin and Brismar, 2004, 2005; Palva et al., 2013; Smit et al., 2011). The ubiquity of LRTC has been further demonstrated by the discovery of its presence in subcortical structures (subthalamic nucleus, (Hohlefeld et al., 2012)). In this paper we consider the effect of *volume conduction* on the estimation of the *Hurst exponents* of both EEG raw electrode data and the EEG amplitude time-series of narrow-band oscillations, but with a particular focus on the latter.

The importance of the LRTC property of amplitude time-series has been elucidated by its relation to hypotheses concerning the optimal functioning of large distributed neuronal networks; this is because on the one hand the LRTC of amplitude time-series has been shown in computational work to coexist with neuronal avalanche activity (Poil et al., 2012), and thus suggests a relationship between oscillatory activity observed in the EEG and the criticality hypothesis (Beggs and Plenz, 2003; Friedman et al., 2012); thus a potential connection between LRTC in the amplitude of oscillations and optimal information processing has been established (Beggs and Plenz, 2003; Shew et al., 2009, 2011). On the other hand, the relevance of the LRTC property to optimal function has been confirmed in clinical studies, where it has been observed that a number of neurological diseases are associated with altered LRTC properties in the amplitude of oscillatory activity including Alzheimer's disease (Montez et al., 2009), schizophrenia (Nikulin et al., 2012), major depressive disorder (Linkenkaer-Hansen et al., 2005) and epilepsy (Monto et al., 2007). The importance of these scale free phenomena

* Corresponding author at: Bernstein Centre for Computational Neuroscience, Berlin, Germany.
E-mail address: duncan.blythe@bccn-berlin.de (D.A.J. Blythe).

http://dx.doi.org/10.1016/j.neuroimage.2014.05.041
1053-8119/

implied by the presence of the LRTC property is further corroborated by numerous fMRI studies (Cabral et al., 2013; Ciuciu et al., 2014; Fox and Raichle, 2007).

The degree of LRTC may be characterized by the magnitude of the *Hurst exponent*, H, whereby values of 0.6–0.8 have been observed as typical in the alpha and beta frequency ranges, across EEG electrodes for healthy subjects (Linkenkaer-Hansen et al., 2001; Nikulin and Brismar, 2004, 2005). Thus studies have pointed towards exponent values which suggest the possibility of universality across subjects.

To date, however, no study has considered whether the observation of LRTC across the scalp is an artifact of either volume conduction or confounding noise sources, or whether the LRTC properties observed in EEG sensor data present a distorted picture of the underlying sources, as has been shown for other quantitative measures, such as measures for connectivity (Meinecke et al., 2005; Nolte et al., 2004, 2008). Thus no consideration has yet been given to the possibility that the LRTC property may be spatially restricted and may only through volume conduction appear in all or many EEG (or MEG) sensors. Conversely no consideration has been given to the possibility that the Hurst exponent values observed in EEG source space may be in fact *higher* than those observed in sensor space, implying the presence of *stronger* dependence properties than previously reported. The validation of such a conjecture would then potentially imply that, for instance, the presence of critical states is heterogeneous across brain regions, or that the diminished values in Hurst exponent measured from the EEG or MEG of patients occur in virtue of attenuation of LRTC in *selected* brain regions.

In this paper we show in simulations, theory and analysis of experimental EEG resting data that an overestimation of the prevalence of LRTC, an underestimation of the largest Hurst exponent present in the source representation of the data *and* an overestimation of the lowest Hurst exponent may occur as a result of mixing effects. *Importantly, the framework we develop, applied to volume conduction, can be equally generalized to the effects of superimposed noise on an LRTC signal.* Thus the measured Hurst exponents in sensor space may be shown in theory and simulations to display *less diversity* than those in source space and to be biased towards the exponents of superimposed noise.

Methods

Hurst exponent estimation

The Hurst exponent H of a time-series $X(t)$ quantifies to what extent information relating to the past history of $X(t)$ is preserved in future samples; if $H = 0.5$ then samples far apart are approximately independent and $X(t)$ is *short-range dependent*.

However if $0.5 < H < 1$ then $X(t)$ is said to be LRTC, with higher values of H denoting a stronger LRTC property; in these LRTC cases, the autocorrelation function of $X(t)$ takes the form of a power-law for large lags:

$$\mathbb{E}(X(t)X(t+\delta)) \sim \frac{\alpha}{\delta^{2-2H}}. \tag{1}$$

Notice that for narrow band oscillatory signals $X(t)$ corresponds to the amplitude envelope of the oscillatory signal and not the raw oscillatory signal. In the analysis of alpha range amplitude dynamics, values of H close to 1 have been found empirically to occur with significant autocorrelations persisting in the amplitude dynamics over thousands of cycles (Linkenkaer-Hansen et al., 2001; Nikulin and Brismar, 2004, 2005).

Testing for the presence of LRTC thus implies measuring H accurately. In principle, using Eq. (1), an analysis of empirical time-lagged correlations should yield an estimate of H. However, in practice, use of the empirical autocorrelations for estimation of H is unreliable, due to the influence of confounding non-stationarities in the low-frequencies of the amplitude dynamics. These non-stationarities, in the raw electrode data, may include, for example, electrode drifts, postural changes or ocular activity.

Thus numerous methodologies have been proposed for the estimation of H to circumvent the difficulties associated with the empirical autocorrelations. In this paper we use two such estimators, viz. Detrended Fluctuation Analysis (DFA) (Peng et al., 1994) and a wavelet estimator using a Daubechies mother wavelet (WD) (Abry and Veitch, 1998; Simonsen et al., 1998). Most importantly, estimation of the Hurst exponent with DFA or WD assumes that our LRTC signals may be modeled as $x(t) + r(t)$ where $r(t)$ is a polynomial trend of fixed degree and $x(t)$ is LRTC with covariance function obeying Eq. (1). DFA and WD are then *invariant* to the presence of $r(t)$ and may be shown to be consistent estimators of the Hurst exponent of $x(t)$ (Bardet and Kammoun, 2007; Moulines et al., 2007). For DFA and WD, log-spaced scales $n_1,\ldots,n_r$ are specified (window lengths) as input, and statistics, resp. $F(n_i)$ and $w(n_i)$ are computed at these scales. For DFA, $F(n_i)$ is computed by first integrating the time-series to get $y(t) = \sum_{i=1}^{t} x(i)$, then detrending $y(t)$ in time-windows of length n_i, to get $\bar{y}_{n_i}(t)$; $F(n_i)$ is obtained by computing the average standard deviation in these time-windows of $\bar{y}_{n_i}(t)$. For WD, $w(n_i)$ is computed by the pyramidal fast wavelet algorithm; high and low pass filters are specified which together constitute a filter bank decomposing $x(t) = a(t) + b(t)$, thus $a(t)$ represents the low-pass component and $b(t)$ the high pass component. This filtering may be applied recursively, substituting at each stage $x(t)$ by $a(t)$ from the previous stage subsampled at every second time point. Thus we obtain time-series $b_{n_i}(t)$ where the n_i is log-2 spaced values. $w(n_i)$ is given as the standard deviation of the time-series $b_{n_i}(t)$. Intuitively both $w(n_i)$ and $F(n_i)$ may be thought of as the level of fluctuation when the time-series is viewed at the scale given by n_i. (See Section A.1 of the Supplementary material for the formal definition of $F(n_i)$.)

One may then show that $w(n_i)$ and $F(n_i)$ scale as n^H. Thus H is estimated by considering the slope of the line of best fit of $\log(n_i)$ against $\log(F(n_i))$, resp. $\log(w(n_i))$.

We choose two separate methods since DFA is well established in the neuroscience literature and achieves high resolution in the frequency domain, while on the other hand, wavelet analysis is computationally efficient and thus proves useful in the optimization procedure we describe in the Spatial filtered Hurst exponent maximization (HeMax) section.

Theory

Mixing effects

When we speak of mixing effects on Hurst exponent estimation, we refer to the difference between the estimated Hurst exponent of a weighted sum $as_1(t) + bs_2(t)$ and the distinct exponents of $s_1(t)$ and $s_2(t)$, or more generally, to the estimated exponent of:

$$x(t) = \sum_{j=1}^{N} c_j s_j(t), \tag{2}$$

as opposed to the exponents of each of the $s_j(t)$.

In this framework we may consider the effects of signal to noise ratio *and* volume conduction on Hurst exponent estimation from the EEG. This is because, for the EEG, signal and noise are superimposed linearly (Haufe et al., 2013; Nikulin et al., 2011), yielding data of the form $s(t) + n(t)$, where $s(t)$ corresponds to the signal and $n(t)$, the noise. For example, $s(t)$ may correspond to a signal displaying a prominent spectral peak in the alpha range, whereas $n(t)$ a signal displaying a power spectrum of $1/f$ form. Moreover, and likewise volume, conduction may be understood as the phenomenon, whereby the data at each electrode is measured as a linear superposition of distinct sources of activity, both signal and noise (Nunez et al., 1997; van den Broek et al., 1998). Thus an electrode recording $x_i(t)$ consists of the sum of weighted activities originating from N distinct sources $s_j(t)$:

$$x_i(t) = \sum_{j=1}^{N} a_{i,j} s_j(t). \tag{3}$$

Notice, however, that a number of the terms $s_j(t)$ may correspond to *noise* (previously denoted $n(t)$). Thus volume conduction and SNR may be considered simultaneously by modeling the electrode recordings as superpositions of signal sources and noise sources. Thus from now on we consider volume conduction and noise in the same framework, viz. as per Eq. (3).

Assumptions

Thus from this point onwards, we assume that the EEG data in sensor space is generated by a mixture of a finite number of sources, both signal and noise. Since these sources are assumed to originate from distinct neural processes, we assume that their dependence is weak. Thus for our simulations and theory we consider independent sources.

Since the sources $s_j(t)$ generating the EEG signal originate from distinct physiological sources, they are each subject to distinct Hurst exponents H_j.

The effect of mixing on estimation of the Hurst exponent of the raw data

The question then arises: what are the Hurst exponents of time-series at the sensors, $x_1(t),\ldots,x_N(t)$ and what does estimation of the Hurst exponents in sensor space (i.e. on the $x_i(t)$) tell us about $H_1,\ldots,H_N$?

Let us first consider the situation in which the *raw signal* is long-range dependent. We show in Section A of the Supplementary material that, if the Hurst exponents of independent time-series $s_1(t)$ and $s_2(t)$ are H_1 and H_2, such that, $H_2 > H_1$ and so that:

$$\mathrm{cov}(s_1(t), s_1(t+\delta)) \sim \frac{\alpha}{\delta^{2-2H_1}} \tag{4}$$

$$\mathrm{cov}(s_2(t), s_2(t+\delta)) \sim \frac{\beta}{\delta^{2-2H_2}} \tag{5}$$

then the Hurst exponent of the weighted sum $as_1(t) + bs_2(t)$ is simply $\max(H_1,H_2)$. *However*, in practice, if the difference $H_1 - H_2$ is not large then we show that the expected value of the DFA-estimated Hurst exponent, H_{DFA}, of $as_1(t) + bs_2(t)$, on finite data, satisfies an approximate relation, as follows: let $f(H) := \frac{(1-H)}{(2+2H)(H+1)(H+2)}$, then,

$$\mathbb{E}(H_{\mathrm{DFA}}) \approx H_1 + \left(\frac{b^2\beta f(H_2)}{b^2\beta f(H_2) + a^2\alpha f(H_1)}\right)(H_2 - H_1). \tag{6}$$

Thus since $a^2\alpha^2 f(H_1) + b^2\beta^2 f(H_2) > b^2\beta^2 f(H_2)$ we have that, on average, the DFA exponent of the sum lies strictly between H_1 and H_2. Since for small $H_2 - H_1$, we have that $f(H_1) \approx f(H_2)$ then, when the weightings of the sum and the asymptotic correlations are equal, i.e. $a = b$ and $\alpha = \beta$, the relation given by Eq. (6) implies that $\mathbb{E}(H_{\mathrm{DFA}}) \approx (H_1 + H_2)/2$.

Mixing and estimation of the Hurst exponent of the amplitude of narrow-band oscillations

A difficulty, however, with the interpretation of the Hurst exponents of the raw data, is that they may be influenced by the filtering properties of the media separating brain and electrode. Thus several papers have argued that these Hurst exponents are of debatable functional significance (Dehghani et al., 2010; Touboul and Destexhe, 2010). Moreover, their measurement is made more difficult by the presence of artifactual activity in the low-frequencies of the raw time-series (polarization potentials, ocular activity etc.). On the other hand, these arguments (of the papers (Dehghani et al., 2010; Touboul and Destexhe, 2010)) which assert the spurious values of Hurst exponents on the raw data *do not apply* to the amplitude time-series of band passed EEG data. This is because for narrow band data the passive filtering properties of the brain tissue are approximately constant and are not likely to explain scaling behavior of the amplitude envelopes. For this reason and also, in addition, since narrowband oscillations such as alpha oscillations and beta oscillations are well studied (Engel and Fries, 2010; Palva and Palva, 2007) in particular with regard to their relevance for brain functionality, we focus in the remainder of the paper on their amplitude time-series, rather than on broad-band raw EEG data. The results obtained for these two bands may easily be generalized to other frequency ranges.

The theoretical analysis, however, when considering narrowband signals possessing LRTC in their amplitude dynamics is, however, different to the raw signal. In this case we model $s(t) = r(t)\cos(\omega t + \epsilon_t)$ where ϵ_t is a random variable with small variance modeling phase slips and $r(t)$ is a slow broad-band time series variable modeling amplitude fluctuations. In particular, we cannot *prima facie* apply the same transforms to derive Eq. (6) to predict the influence of mixing on the values of estimated Hurst exponents. This is because the Hilbert transform and the following rectification of the analytic signal represent a non-linear transform of the narrow-band time-series. Since the sum of two narrowband signals at a single frequency is also narrowband at that frequency (consider Fourier representation), then we are interested in the estimated Hurst exponent of $q(t)$ where:

$$q(t)\cos\left(\omega t + \epsilon_{3,t}\right) = r_1(t)\cos\left(\omega t + \epsilon_{1,t}\right) + r_2(t)\cos\left(\omega t + \epsilon_{2,t}\right). \tag{7}$$

Eq. (6) is derived by considering the Hurst exponent of broadband *raw* signals. We are now interested in the relationship between the Hurst exponents of the amplitudes $q(t)$ and $r_1(t)$,$r_2(t)$. (Note that r_1 and r_2 can also be considered as signal and noise, respectively. Therefore the same logic should be applied to the effects of volume conduction and SNR.) Thus a straightforward application of Eq. (6) is not possible since Eq. (6) gives the expected Hurst exponent estimate of $y(t) = as_1(t) + bs_2(t)$, for scalars a,b, but this relationship does not hold between $q(t)$ and $r_1(t)$ and $r_2(t)$ when we sum the underlying oscillatory signals as per Eq. (7). Thus, $r_1(t)$ is the Hilbert transform of $s_1(t)$, which we denote, $H(s_1(t)) = r_1(t)$, and similarly for $r_2(t)$; however, a direct application, in this scenario, of Eq. (6) would require that $H(s_1(t) + s_2(t)) = H(s_1(t)) + H(s_2(t))$, which does not hold in general.

However, under the assumption that the amplitude time-series are approximately Gaussian, we are able to apply theoretical arguments (Section B.2 of the Supplementary material) relating the behavior of scaling to mixing of oscillatory sources which imply that the estimated Hurst exponent of the sum of two oscillatory sources lies between the Hurst exponent of each source. Moreover, we check in the simulations of the following section that Eq. (6) provides a useful prediction for the measured exponent on the amplitude of the mixture of two signals provided H_1 and H_2 are not significantly different. Notice, however, that our simulations *do not* assume Gaussianity. However, we show that the theoretical results which assume Gaussianity yield a useful prediction for non-Gaussian amplitudes.

The theoretical argument, in summary, shows that the scaling exponent of the amplitude of narrowband oscillations is related to the variance *of the sample variance* estimate of the oscillatory signal. Under the assumption that the amplitude of the oscillations is LRTC Gaussian processes, we may moreover show that the variance *of the sample variance* scales log-linearly in data points and proportionally to H. Since, under the assumption of independence of sources, the variance *of the sample variance* also distributes under addition of narrow-band sources, we arrive in a situation analogous to Eq. (6), which leads to the fact that the exponent of a sum of sources lies between the exponent of the individual sources (technical details are provided in the Supplementary material, Sections B1 and B2).

Simulations

In this section we describe simulations involving *narrowband* signals possessing LRTC amplitude dynamics. For the analysis of the simulated data, we extract the amplitude of the signal via the Hilbert transform and use DFA to estimate the Hurst exponents in each case. For all

simulations the following parameters apply: $T = 200,000$ (no. of time-points), $d = 1$ (DFA detrending degree), and 20 evenly log-space values for n in the range 1000,…,50, 000.

Method of simulation of LRTC oscillatory sources

In order to generate LRTC oscillatory sources, we use the Kuramoto model (Kuramoto, 2003); in this way we are able to generate oscillations whose amplitude time-series are LRTC in a principled fashion, avoiding ad hoc constructions, whereby the phase and amplitude of the signal are sampled separately[1]. Thus we generate samples according to the following model, for $i = 1,\ldots,N$ and where the $\xi_i(t)$ is uncorrelated Gaussian processes:

$$\frac{\partial \phi_i}{\partial t} = D\xi_i(t) + \omega_0 + \frac{\kappa}{N}\sum_{j\neq i}\cos\left(\phi_i(t) - \phi_j(t)\right).$$

The parameter D controls the noise strength, κ controls the strength of synchrony between the oscillators ϕ_i and ω_0 denotes the basic oscillatory frequency of the ensemble. In order to measure the joint behavior of all N oscillators one considers the *mean field* of the ensemble, viz.:

$$M = \frac{1}{N}\sum_{j=1}^{N}\exp\left(i\phi_j(t)\right).$$

Thus full synchrony in the ensemble is achieved when $|M| = 1$ whereas in the asynchronous regime $|M| \to 0$ as $N \to \infty$. For a fixed connectivity strength κ, which regime the ensemble occupies is determined by the noise strength D (see the Method of simulation of LRTC oscillatory sources section for a description of the model and the parameters). Most importantly for our purposes, when D is chosen so that the ensemble approaches the phase transition between synchrony and asynchrony, then the measured Hurst exponents of $|M|$ imply LRTC, and, moreover, the real part of M is approximately narrow band due to the fact that each individual oscillator shares the same carrier frequency, and the fact that the noise strength is insufficient in proportion to the connectivity to force significant contributions at frequencies differing from ω_0 to remain negligible. Note that this approach to generating oscillatory sources with fluctuations in their amplitude dynamics was recently applied by Deco et al. (Cabral et al., 2013).

Addition of pairs of amplitude-LRTC sources

In the current section, we simulate pairs of amplitude-LRTC oscillatory sources subject to varying Hurst exponents, which we control via the noise parameter D; the remaining parameters are taken as follows: $\kappa = 0.1$, $N = 80$, $\omega = 40$, and $dt = 0.01$. In particular we take pairs of oscillatory sources $s_1(t)$ and $s_2(t)$ (modeling equally two oscillatory sources volume-conducted to the sensors or a signal and noise superposition) over a grid of values D_1 and D_2 implying that we measure H_1 and H_2 in the range 0.5,…,1. We measure the Hurst exponent using DFA for $s_1(t)$, $s_2(t)$ and $s_1(t) + s_2(t)$.

The effect of SNR

In the current section we simulate an amplitude-LRTC oscillatory signal as before, superimposed by a noise signal at SNRs ranging between 2^7 and 2^{-7}. For the LRTC source, we set $D = 7.8$. The noise source is generated by filtering Gaussian white noise in the alpha range, yielding a Hurst exponent for the amplitude dynamics of $H = 0.5$. The Hurst exponents are measured as in the previous simulation (the Addition of pairs of amplitude-LRTC sources section).

[1] Such an ad hoc procedure leads to spurious high frequency artifacts due to the fact that the phase and amplitude do not arise from a single generative process.

Simulation of mixing of cortical LRTC sources using an EEG forward model

In this simulation we use an EEG forward model calculated on the basis of the MRI scans of 152 human participants (Fonov et al., 2011) and implementing a forward mapping from simulated dipoles to voltages at the electrodes computed using the semi-analytic methods of Nolte and Dassios (2005). The electrode placement is chosen as analogous to the placement in the EEG data we study later in the paper. We simulated 10 alpha sources with LRTC amplitude dynamics over a range of Hurst exponents between 0.5 and 1. These were placed randomly in the cortex with 76 noise sources whose amplitude dynamics displayed no LRTC ($H = 0.5$), placed randomly throughout the model-brain. Thus as many sources as electrodes (80) were generated. We set the signal to noise ratio to 0.4, where the SNR was measured as the ratio of average variance per source in the alpha range of the LRTC sources to the average cumulative variance in same range over *all* non-LRTC sources, measured on average in sensor space. The Hurst exponents were measured with DFA in sensor and source space. This simulation was repeated 100 times and the mean, kurtosis and skewness of the empirical distribution obtained by pooling all exponents were measured in source/component and sensor space.

Notice that we include a further iteration of this simulation, checking for the effects of electrode density in Section C of the Supplementary material.

Source representations

In this section we discuss techniques for computation of a plausible source representation in which the Hurst exponents of the amplitude of neuronal oscillations may be calculated. The most appropriate method should allow us to more reliably calculate the value of the largest and smallest Hurst exponents present in the multivariate data.

Spatial filtering

The most straightforward source representations we apply are obtained via Laplacian and bipolar spatial filtering (Srinivasan et al., 1996); in this representation spatial smearing or volume conduction effects between recordings at sensors are reduced by moving to sources which are obtained by subtracting from each electrode a weighted sum of neighboring electrodes, which computes a high-pass spatial filtering (Graimann and Pfurtscheller, 2006). We apply this spatial filtering in 3 variants; in the first variant a sum of surrounding channels are subtracted (Laplacian), in the remaining variants, we calculate resp. transverse and longitudinal bipolar derivations. The advantages of this approach are its simplicity and low computational complexity. Disadvantages include the fact that the number of sources obtained is less than the number of channels recorded and that no consideration is taken of the subject specific information present in the data.

TDSEP

The most broadly used source separation technique in EEG data analysis is independent components analysis (ICA), of which numerous variants exist (Hyvärinen and Oja, 2000). We apply TDSEP (Ziehe and Müller, 1998; Ziehe et al., 2004), a variant of ICA which uses time-lagged autocorrelations, since the neural sources often exhibit limited non-Gaussianity, upon which alternative ICA methodologies, based on higher order-statistics, are based. The advantage of this method is that only the time-lags need be specified as parameters and that the method is robust to Gaussianity of the underlying sources. The disadvantages of the method include sensitivity to, in particular, motion artifacts, as is the case for most ICA algorithms; in fact, TDSEP is often used exactly to identify these artifacts. In the present study only weak movement artifacts are present due to the fact that we study EEG in the resting state. Thus the power of TDSEP to identify oscillatory sources may be limited for datasets contaminated by stronger artifactual components. Another important limiting factor is the spectral similarity of many oscillatory sources. Given that TDSEP favors components with different spectra,

similar frequency content of neuronal signals may lead to components combining the activities of different sources.

Spatial–spectral decomposition (SSD)

We consider a source separation procedure, spatio-spectral decomposition (SSD) (Nikulin et al., 2011), which explicitly calculates a source representation which optimizes for oscillatory sources. In particular SSD computes a basis of sources which are ordered in such a way that the signal to noise ratio in a frequency band of interest is maximized; the SNR is measured by considering the ratio of power in the frequency band of interest to the power in the flanking frequencies. The advantages of this method include its low computational efficiency (solvable as a generalized eigenvalue problem) and the fact that the method can be configured to optimize for signal to noise ratio in the frequency band in which LRTC is measured. On the other hand, there is no guarantee that SSD results in sources maximizing independence between the respective sources.

Spatial filtered Hurst exponent maximization (HeMax)

Finally, in order to gain insight into the correct source representation we present a novel algorithm which we term spatial filtered Hurst exponent maximization or *HeMax*. The algorithm *explicitly* optimizes a spatial filter $\mathbf{w}$ so that the estimated Hurst exponent of the amplitude dynamics in the alpha range of the spatially filtered data $\mathbf{w}^\top\mathbf{x}(\mathbf{t})$ is maximized.

In summary, we define a loss function $\mathcal{L}(\mathbf{w},\mathbf{x}(\mathbf{t}))$ whose output is the estimated Hurst exponent under the spatial filter $\mathbf{w}$, using a wavelet estimator with a Dauchechies mother wavelet of order 6. We then compute the derivative of this objective function and optimize by gradient descent.

Our motivation in deriving and presenting this method is that there is no a priori reason for believing that the source separation algorithms TDSEP and SSD are suitable for obtaining optimal source approximations with respect to obtaining Hurst exponent values corresponding to the values of the underlying neural processes. We may use HeMax to test whether these methods are suitable for this purpose, since we know from our theory that a time series obtained by spatial filtering with maximal Hurst exponent cannot be a mixture of multiple sources.

The details of the method are given in Section B.4 of the Supplementary material, and the algorithmic flow is summarized in Algorithm 1.

Algorithm 1. HeMax (Supplementary material B.3)

1: The analytic signal is computed for each channel of the multivariate EEG data. (Step 2, Section B.3).
2: **while** True **do**
3: The analytic signal data is projected by the spatial filter $\mathbf{w}$. (Section B.3, Equation (6))
4: Mallet's fast wavelet transform is computed on the data. (Step 4, Section B.3; Equation (6)).
5: The objective function value is evaluated by log regression on the wavelet coefficients (Equation (6), Section B.3).
6: **if** Obj. fun. increase is insufficient **then**
7: Break
8: **else**
9: The gradient is computed and $\mathbf{w}$ and the analytic signal data are updated so as to yield an increase in the estimated Hurst exponent. (Step 5, Section B.3; Equations (8),(9),(10)).
10: **end if**
11: **end while**

Analysis of real EEG data

In this section we compare Hurst exponents calculated in source and sensor space from real EEG data. Seven subjects participated in the study (1 female). The experimental protocol was approved by the Institutional Review Board of the Charité, Berlin. EEG recordings were obtained at rest with subjects seated comfortably in a chair with their eyes open. Recordings were made during three sessions of 5 min each, with each data set thus comprising altogether roughly 15 min of data. EEG data were recorded with 96 Ag/AgCl electrodes, using BrainAmp amplifiers and BrainVision Recorder software (Brain Products GmbH, Munich, Germany). The signals were recorded in the 0.016–250 Hz frequency range at a 1000 Hz sampling frequency.

The data analytic steps taken were as follows:

Outlier channels were rejected after visual inspection for frequent shifts in voltage and poor signal quality. The data was then re-referenced according to the common average and filtered forwards and backwards using a fourth order Butterworth filter in the alpha range (8 to 12 Hz).

Following these preprocessing steps, the amplitude envelopes of the oscillatory signal were computed in sensor space using the Hilbert transform and the Hurst exponents were computed as per the

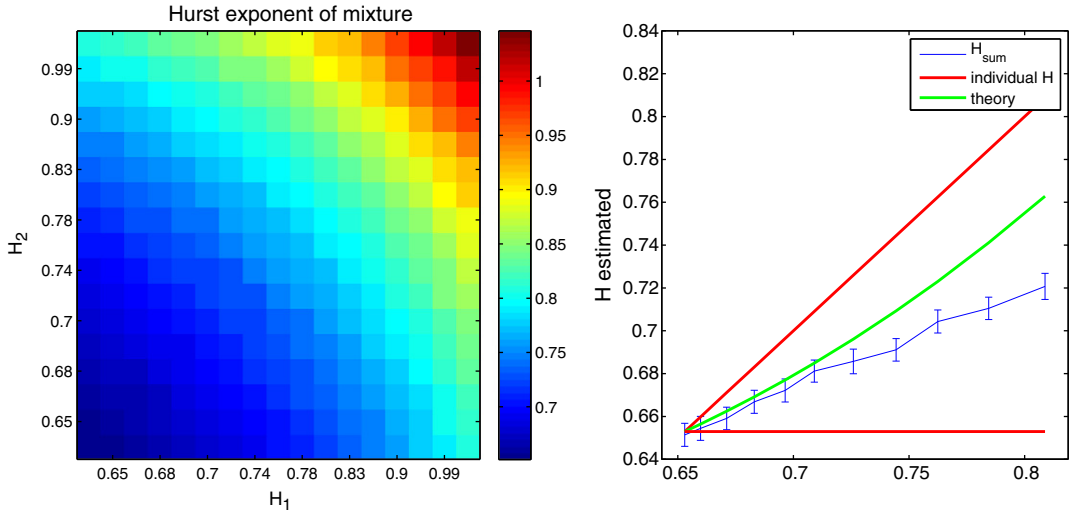

Fig. 1. Simulation of DFA estimated Hurst exponents of mixtures $s_1(t) + s_2(t)$ versus the individual sources; 1000 pairs of oscillatory sources were generated at varying noise levels from the Kuramoto model, yielding pairs with Hurst exponents H_1 and H_2 between 0.6 and 1. The estimated Hurst exponents of the sum lies between the exponents of the individual sources (left). Moreover for sources whose Hurst exponents are close to one another, the estimated Hurst exponent of the sum is well predicted by the theoretical result of Eq. (6) (right hand panel).

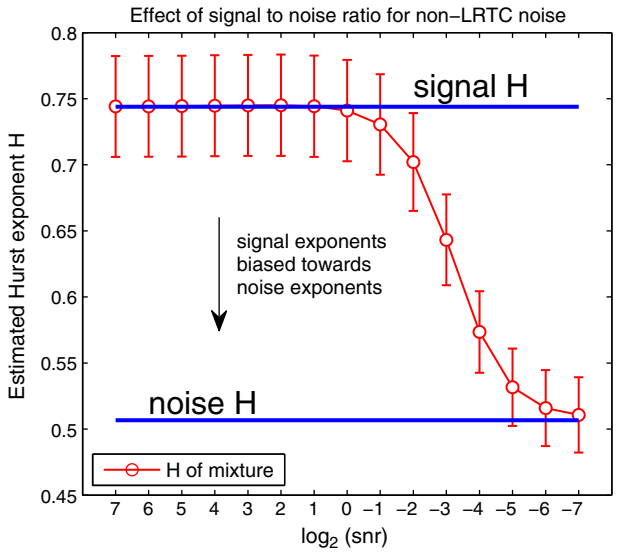

Fig. 2. Simulation (described in The effect of SNR section) demonstrating the effect of signal to noise ratio on estimation of the Hurst exponent of the underlying signal.

Addition of pairs of amplitude-LRTC sources section but applying detrending of polynomial degree, $d = 5$ (we used a more conservative detrending for the experimental data, to ensure that results do not depend on artifactual influence).

Subsequently 3 varieties of spatial filter (Laplacian and 2 bipolar) were computed (see the Spatial filtering section) and applied these to the preprocessed sensor space data, and on the amplitude of this Laplacian filtered data Hurst exponents were computed as before using DFA.

After these steps the dimensionality of the (originally preprocessed) data was reduced by 1 using PCA $s_{pca}(t) = W_{pca}x(t)$ in order to compensate for the rank reducing effects of common average referencing.

Then sources were computed with TDSEP ($s_{tdsep}(t) = W_{tdsep}s_{pca}(t)$) and SSD ($s_{ssd}(t) = W_{ssd}s_{pca}(t)$); sources with artifactual topographies or power spectra were rejected and the Hurst exponents of the amplitude of the computed components were estimated using DFA.

Finally, the 10 SSD sources displaying the largest signal to noise ratio in the alpha range were selected and a further linear spatial filter was computed using HeMax maximizing the wavelet-estimated Hurst exponent in the alpha range (Daubechy wavelet order = 6) as described in the Simulations section ($s_{\max}(t) = w_{\max}s_{ssd}(t)$. The Hurst exponent was estimated on the calculated source using DFA as before.

Results

Simulations and theory

Addition of pairs of amplitude-LRTC sources

The results of the simulation described in the Addition of pairs of amplitude-LRTC sources section are displayed in Fig. 1. The left panel displays all Hurst exponents measured, and the right hand panel demonstrates that for H_1, H_2 not significantly different, we observe agreement between the prediction made by Eq. (6) and the empirical results. For the range of D (noise strength) considered, we find H_1 and H_2 to lie between approx. 0.6 and 1. Further simulations (not presented here) suggest that similar behavior extends to the range 0.5 to 1. We may conclude that for H_1 and H_2 between 0.5 and 1, the DFA-measured Hurst exponent of $s_1(t) + s_2(t)$ lies strictly between H_1 and H_2. By transitivity this will imply that for an arbitrary sum of sources, the measured Hurst exponent of the sources will lie *between* the largest and smallest exponent of the sources participating in the sum. This conclusion holds for the summation of two signals and for a summation of signal and noise.

The effects of SNR

The results of the simulation described in the Effect of SNR section are displayed in Fig. 2. The figure shows that with decreasing SNR, the estimated Hurst exponent of the signal is biased towards the exponent

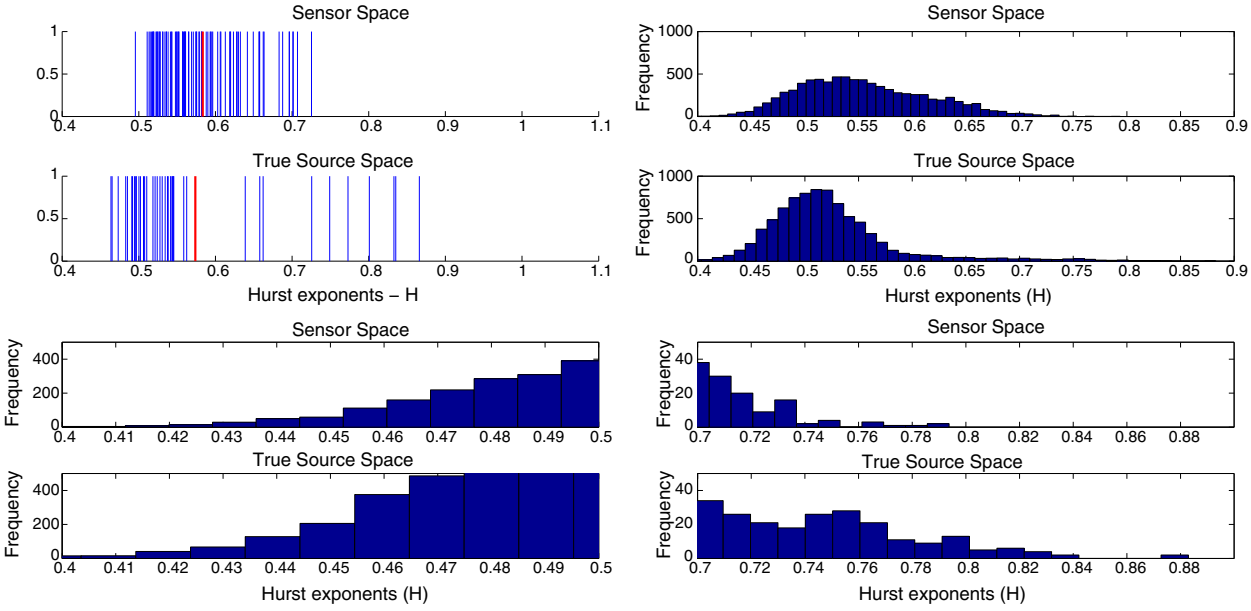

Fig. 3. The figure displays results of computing Hurst exponents on narrowband oscillations when the mapping between sources and sensors is computed using an EEG forward model. On the left, the individual exponents on resp. sensors, sources are displayed (each blue line denotes one exponent) for one realization of the data setup. The mean in each representation is displayed in red. On the right the exponents are displayed over 100 realizations of the data setup as a histogram for resp. sensor and source space. The estimates of Hurst exponents in sensor space (upper panel) are biased towards the mean of exponents (lower panel), in the sense that the largest exponents and smallest exponents in sensor are closer to their mean than in source space; moreover, the mean in sensor space overestimates the mean in source space and the range over exponents in sensor space is drastically lower than in source space. The kurtosis and skewness in source space are significantly larger (on average resp. 187% and 317% larger) than in sensor space. To confirm the behavior in the tails of the top right panels we present blown up visualization of the tails in the bottom row. See the Simulation of mixing of cortical LRTC sources using an EEG forward model section for details.

of the noise (in this case ≈0.5). Notice however, that noise sources need not be uncorrelated, such that $H = 0.5$. We show in Section D.2 of the Supplementary material that non-oscillatory frequency bands of resting state EEG data (i.e. noise sources) may also exhibit LRTC dynamics. In such cases, further simulations show that the qualitative effect of SNR is identical, i.e. the exponents of the signal are nevertheless biased towards the exponents of the noise sources.

Simulation of mixing of cortical LRTC sources using an EEG forward model

The results of the forward model simulation described in the Simulation of mixing of cortical LRTC sources using an EEG forward model section are displayed in Fig. 3 and show that the largest exponent in sensor space is smaller than the largest in source space, and likewise the smallest in source space is smaller than the smallest in sensor space; we observe a diminished range in exponents in source space, with apparent LRTC visible in *all* sensors. Moreover, the kurtosis and skewness over all exponents are resp. 187% and 317% greater in source space than sensor space and the mean in sensor space is 6% larger than the mean in source space.

Notice that in Section C of the Supplementary material, we find that increasing the number of electrodes beyond approximately 50 electrodes has little effect on the results. Thus increasing electrode density in sensor space does not serve to diminish the problems posed by SNR and volume conduction.

Implications/predictions of the simulations and theory

The simulations and theory show that:

1. The addition of 2 independent sources with identical Hurst exponents yields a source whose measured exponent lies between the larger and the smaller of the exponents of the individual components (the Addition of pairs of amplitude-LRTC sources section).
2. If LRTC narrowband sources are mixed with random noise by means of an EEG forward model, then the exponents measured in sensor space are biased towards values which do not reflect the distribution of exponents in the true sources; the largest exponent measured in sensor space is smaller than the largest in source space; the smallest exponent measured in sensor space is larger than the smallest measured on the true sources.

Thus, as a result of our theoretical considerations and simulations, we find the following to be true:

If the maximum and minimum Hurst exponents in source space are $H^s_{\max} > H^s_{\min}$ *and in sensor space:* $H^x_{\max} > H^x_{\min}$*, then:*

$$H^s_{\min} \leq H^x_{\min} < H^x_{\max} \leq H^s_{\max}.$$

EEG data

In Fig. 4 we display the results of calculating the exponents for all subjects in sensor space and each of the source representations discussed in the Source representations section and in Fig. 5 we present the exponents by subject. The results of Fig. 4 show that all source representations generate a wider diversity than the sensor space representation in their distribution over measured exponents when all subjects are considered — the variance over exponents is in each case significantly greater than in source space (two-sided *f*-test) and the mean and median over exponents in sensor space significantly *overestimate* the corresponding statistics in source space (two sided *t*-test; Wilcoxon sign-rank). Moreover, the mean over subjects of the difference between the largest exponent in the TDSEP representation and the largest in sensor space is significantly greater than zero (two-sided *t*-test). The results of Fig. 5 show that the minimum exponent in source space for all representations is smaller than the minimum in sensor space for *all* subjects and the mean of the minimum is significantly smaller (two-sided *t*-test). Finally one observes that the higher order statistics (when considering the distribution of exponents) of the source representations imply more pronounced non-Gaussianity than those of the sensor space representations: in all cases, with the exception of the skewness of the small Laplacian derivation and the kurtosis of the vertical Laplacian derivation, we find that the skewness and kurtosis of the exponents in each of the source representation are significantly greater than the corresponding statistics in sensor space (1000 bootstrap iterations). This is in complete agreement with the findings of the EEG forward model simulation (the Simulation of mixing of cortical LRTC sources using an EEG forward model section). All *p*-values are displayed in Table 1.

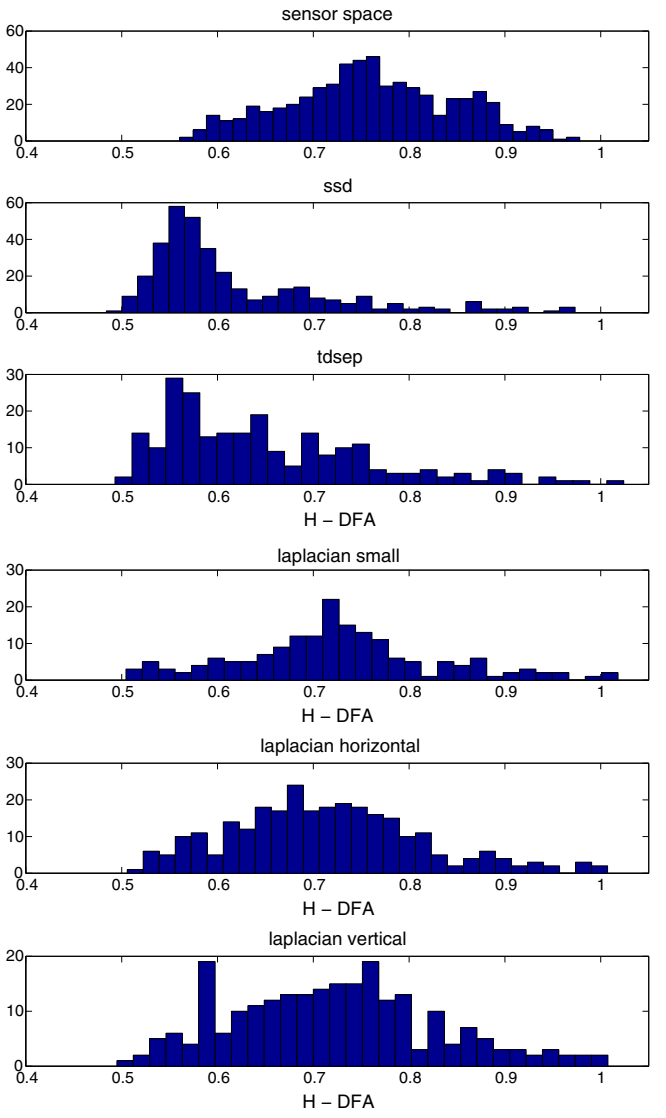

Fig. 4. The figure displays in each panel the empirical distribution as a histogram of all DFA-estimated Hurst exponents in resp. sensor space and SSD, TDSEP and Laplacian (3 variants) source spaces. The results show that the distribution in SSD and TDSEP source spaces have greater variance, range, lower mean, higher kurtosis and higher positive skewness than in sensor space.

In Fig. 6 we present scalp maps resulting from the optimization procedure outlined in the Spatial filtered Hurst exponent maximization (HeMax) section above. In each case we display the pattern obtained by optimization and the most similar SSD and TDSEP patterns. The results show a high degree of similarity between the SSD and TDSEP patterns and the maximized exponent pattern. Note that in general the topographies correspond to the typical maps of alpha oscillations

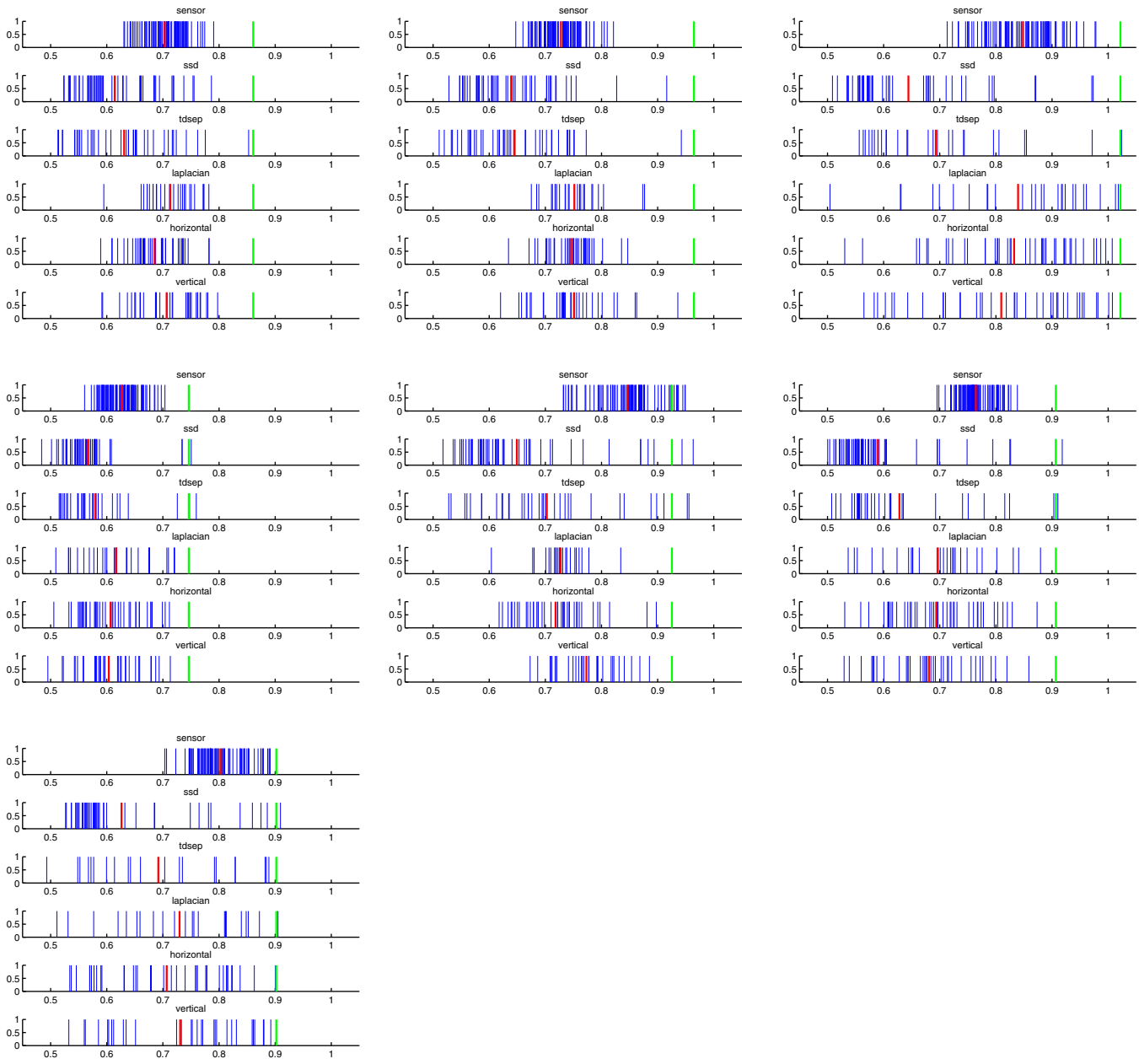

Fig. 5. The figure displays the individual Hurst exponents obtained in resp. sensor space and SSD, TDSEP and Laplacian (3 derivations). For each subject the magnitude of the Hurst exponent on each sensor or source, resp. is displayed by a blue line. Each subplot for each subject corresponds, resp. to either a sensor space, or an approximation to source space (SSD, TDSEP etc.). The mean over measurements is displayed in red and, for comparison, the DFA measured exponent of the source obtained by optimization of the wavelet-estimated Hurst exponent is displayed in green. The results show that both SSD and TDSEP are competitive with the maximization procedure, and in most cases find a representation whose measured largest Hurst exponent exceeds the corresponding value in sensor space. Moreover, in each case SSD and TDSEP finds a source whose Hurst exponent is smaller than any measured in sensor space and in all cases, the range of the SSD and TDSEP Hurst spectrum exceeds the range in sensor space.

generated in occipito-parietal and central areas (mu rhythm). This confirms that SSD and TDSEP are suitable in the context of resting state EEG for elucidating the range of Hurst exponents characterizing source space.

Discussion and conclusion

In this paper we presented theory and simulations which show that mixing effects may lead to significant differences in estimated Hurst exponent values in source and sensor space. The obtained predictions were confirmed in simulations and analyses of real resting state EEG data.

Previous results on the existence of LRTC are not spurious

The first encouraging result of our simulations, theory and data analysis is that the LRTC observed in sensor space is not an artifact of volume conduction or confounding noise; if we observe LRTC in sensor space, then sources must be present which display LRTC. This is because the Hurst exponents of a mixture lie *between* the exponents of the sources forming the mixture. More precisely: *it is not possible by mixing sources with white-noise exponents ($H = 0.5$) to obtain a signal with exponent exceeding 0.5 regardless of the weighting factors.* Moreover the fact that increasing the SNR in the alpha range via the application of SSD confirms that the LRTC property resides primarily in the *signal* and not the linearly superimposed noise.

Table 1
p-Values for differences in distribution in the respective source representations vs. sensor space.

	Variance	Median	Mean	Max. mean	Min. mean	Skew.	Kurt.
SSD	0.0464	≪0.0001	≪0.0001	0.0592	0.000544	≪0.0001	≪0.0001
TDSEP	≪0.0001	≪0.0001	≪0.0001	0.0164	0.000926	≪0.0001	0.0002
Laplacian small	0.0042	≪0.0001	≪0.0001	0.78	0.0376	0.065	0.0032
Laplacian horizontal	0.0062	≪0.0001	≪0.0001	0.570	0.0136	0.0004	0.007
Laplacian vertical	≪0.0001	≪0.0001	≪0.0001	0.402	0.0128	0.016	0.232
H optimization	–	–	–	0.0428	–	–	–

In each case we perform a two-sided, two-sample test for equality of distribution using the statistics displayed in the first row. See the EEG data section for details.

Thus the existence of LRTC in the amplitude dynamics of neuronal oscillations, asserted by numerous previous contributions (Linkenkaer-Hansen et al., 2001; Nikulin and Brismar, 2004; Nikulin and Brismar, 2005; Palva et al., 2013; Smit et al., 2011), does not require revision.

Previous quantitative assessments of the Hurst exponent on EEG data require revision

The *quantitative* differences observed in sensor and source space are *pronounced*; thus results derived in EEG (MEG) sensor space deserve further attention in the light of this observation, given that an interpretation in sensor space of Hurst exponent values may lead to erroneous conclusions. Thus although we may safely conclude that LRTC is present on the basis of existing results, the exact configuration of this LRTC in source space requires further investigation.

The dangers of ignoring the effects of volume conduction have already been acknowledged in the connectivity literature. We hope to avert similar misinterpretations in the emerging domain of long-range dependence analysis by bringing the effects of volume conduction on Hurst exponent estimation to the EEG/MEG community's attention.

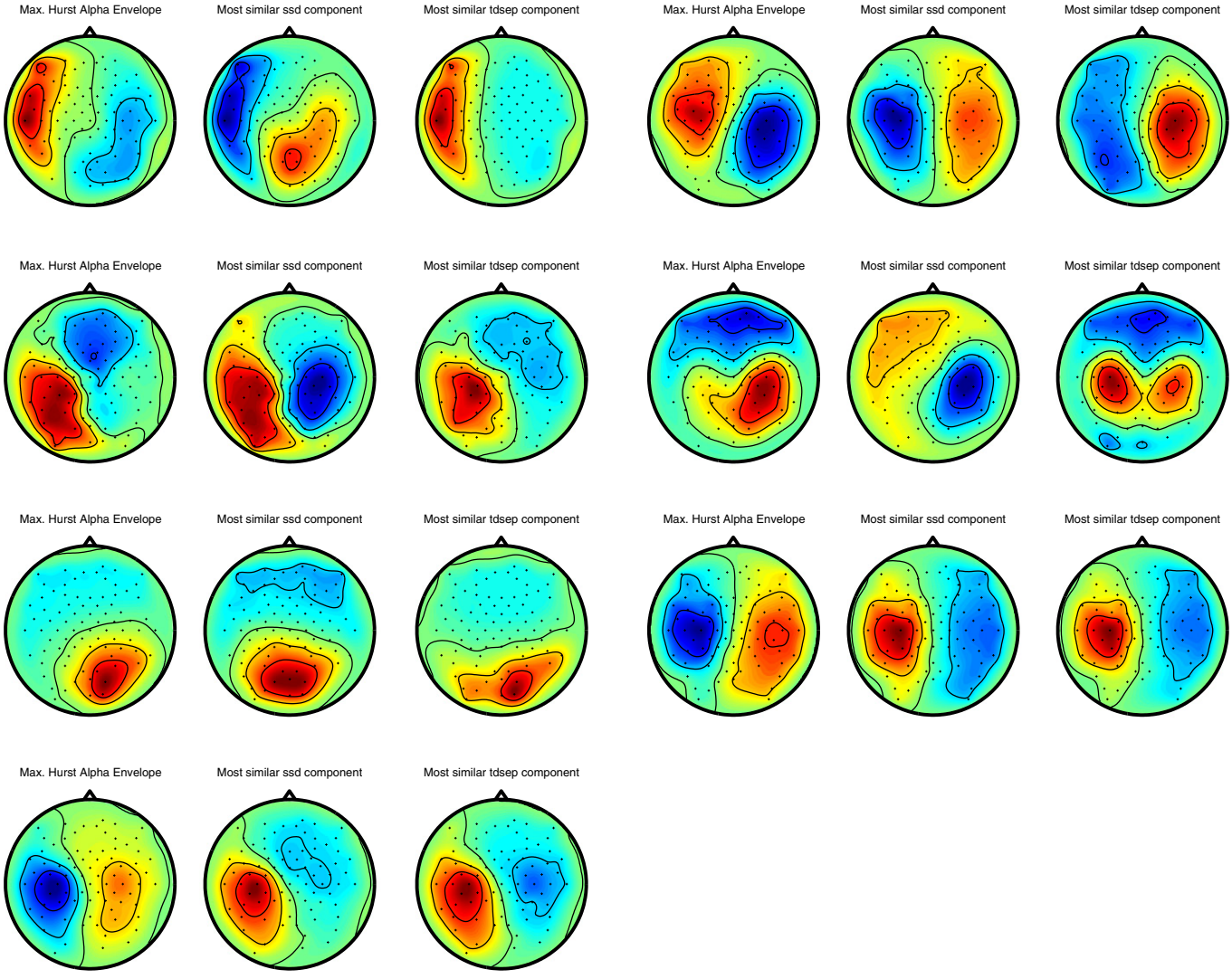

Fig. 6. The figure displays the spatial patterns obtained by maximization of the wavelet-estimated Hurst exponent under a spatial filter and the most similar TDSEP and SSD patterns. The results show a high degree of similarity between the optimized pattern and each of the TDSEP and SSD patterns. Thus each panel denotes the results obtained on one subject and the right hand panels display resp. the most similar TDSEP and SSD patterns. The results confirm that both TDSEP and SSD yield close to optimal representations for the study of the source activities exhibiting the largest Hurst exponents, since the pattern obtained by optimizing the magnitude of the estimated Hurst exponent under the corresponding filter is similar to patterns belonging to the TDSEP or SSD representations.

No evidence for universality of Hurst exponent values across the scalp

Our analysis shows that an unwarranted conclusion, which is tempting when only looking at sensor space, is to interpret the narrow range of exponent values in sensor space as evidence for universal dynamical system properties, as has been argued on the basis of neuronal avalanche exponents (Poil et al., 2012). However, consideration of source space exponent values lends less support to this thesis: in source space we observe a wide range of exponent values, with exponent values close to the exception rather than the norm. Thus the wide range of Hurst exponents observed in source space allows for the possibility that *only a subset* of distributed neuronal networks exist in a regime which generates LRTC amplitudes in oscillations. *However*, notice that this remains only a *possibility*; an alternative explanation for the wide range of exponents in source space is that we observe amplitude time-series *in source space* at varying SNRs. Thus oscillations *may* be in fact subject to Hurst exponents close to $H \approx 1$, but we measure these oscillations confounded by noisy non-LRTC components in source space. Support for this scenario in the alpha range is provided by the observation that the highest values of H observed correspond to oscillations with the highest SNRs (visual alpha and mu). Moreover, in our simulations we showed that decreasing SNR shifts the scaling exponents towards the exponents of the noise ($H = 0.5$).

The use of Hurst exponents as experimental observables requires revision

A further context which must be reconsidered with respect to source representations vs. sensor space is in the use of Hurst exponent values as experimental observables. For instance, numerous studies of pathological EEG have used Hurst exponents as a basis for distinguishing between neurological or psychiatric patients (P) and healthy controls (C) (Linkenkaer-Hansen et al., 2005; Montez et al., 2009; Monto et al., 2007; Nikulin et al., 2012). In such a scenario, focusing on source space should yield greater statistical power, since if a certain small subset of sources present in the EEG of subjects in *P* possess lower Hurst exponents than in *C*, then this difference may only be clearly visible in source space. In sensor space due to the measurement of superpositions of sources, caused by volume conduction, small exponents may not be observable at all. Moreover, even if the difference in *P* and *C* is visible in sensor space, if this discrepancy is due to certain specific sources, then the use of decomposition techniques should yield more detailed physiological hypotheses, differentiating for instance between contributions from sensory and higher order brain areas in psychiatric disorders, such as schizophrenia. In another scenario, it might be the case that all sources of subjects in *C* possess slightly larger exponent values than most sources of subjects in *P*, but a few selected sources of subjects in *P* possess very high exponent values, with the result that no difference between *P* and *C* is visible in sensor space, although highly significant differences exist at source level (due volume conduction effects). Such potential misinterpretations must be respected and avoided. Over and above comparing groups of subjects (such as patients and healthy controls), similar logic may also be applied for comparing scaling exponents between experimental conditions, for instance comparing neuronal dynamics at rest and during a task. All the abovementioned peculiarities in the expression of exponents in sensor space, as opposed to sources space, are readily applicable to this comparison. (To check the relevance of our study in these contexts we present analysis of the data from one stroke patient in Section C of the Supplementary material, where we see that the same predictions from our theory and simulations apply.)

SSD, TDSEP and HeMax may be used to study Hurst exponent values from resting state EEG

We presented above, a new method for optimizing spatial filters from empirical EEG data, viz. *HeMax*. The algorithm proved useful, for the resting state EEG analysis, by demonstrating that SSD and TDSEP succeed in obtaining source activities which correspond to activities with maximal Hurst exponent. Further work is required to show that SSD and TDSEP are suitable for a range of paradigms. In such cases, a comparison using HeMax is necessary.

Conclusion

In conclusion, as well as providing a mathematical and critical assessment of volume conduction and SNR effects on the expression of scaling exponents in EEG/MEG sensor space, we also advocate the use of spatial decomposition techniques for a more reliable quantification of LRTC in the amplitude dynamics of neuronal oscillations. Future studies will focus on analyzing task based paradigms as well as clinical data sets using a source based Hurst exponent analysis.

Acknowledgments

The authors would like to thank Daniel Bartz for his valuable input in discussions. DAJB was supported by a grant from the German Research Foundation, research training group GRK 1589/1 “Sensory Computation in Neural Systems”. SH acknowledges support by the German Federal Ministry of Education and Research (BMBF), grant no. 01GQ0850. KRM was supported by EU, BMBF, DFG and the Brain Korea 21 Plus Program through the National Research Foundation of Korea funded by the Ministry of Education, Republic of Korea. VVN was partially supported by the Berlin Bernstein Center for Computational Neuroscience (BCCN 01GQ 1001C) and by the Basic Research Program of the National Research University Higher School of Economics.

Appendix A. Supplementary data

Supplementary data to this article can be found online at http://dx.doi.org/10.1016/j.neuroimage.2014.05.041.

References

Abry, P., Veitch, D., 1998. Wavelet analysis of long-range-dependent traffic. IEEE Trans. Inf. Theory 44, 2–15.
Bardet, J.-M., Kammoun, I., 2007. Asymptotic properties of the detrended fluctuation analysis of long range dependent processes. IEEE Trans. Inf. Theory 54, 2041–2052.
Beggs, J., Plenz, D., 2003. Neuronal avalanches in neocortical circuits. J. Neurosci. 23, 11167–11177.
Cabral, J., Luckhoo, H., Woolrich, M., Joensson, M., Mohseni, H., Baker, A., Kringelbach, M., Deco, G., 2013. Exploring mechanisms of spontaneous MEG functional connectivity: how delayed network interactions lead to structured amplitude envelopes of band-pass filtered oscillations. NeuroImage 90, 423–435.
Ciuciu, P., Abry, P., He, B.J., 2014. Interplay between functional connectivity and scale-free dynamics in intrinsic fMRI networks. NeuroImage 95, 248–263.
Dehghani, N., Bédard, C., Cash, S., Halgren, E., Destexhe, A., 2010. Comparative power spectral analysis of simultaneous elecroencephalographic and magnetoencephalographic recordings in humans suggests non-resistive extracellular media. J. Comput. Neurosci. 29, 405–421.
Engel, A.K., Fries, P., 2010. Beta-band oscillations—signalling the status quo? Curr. Opin. Neurobiol. 20, 156–165.
Fonov, V., Evans, A., Botteron, K., Almli, C., McKinstry, R., Collins, D., 2011. Unbiased average age-appropriate atlases for pediatric studies. NeuroImage 54, 313–327.
Fox, M.D., Raichle, M.E., 2007. Spontaneous fluctuations in brain activity observed with functional magnetic resonance imaging. Nat. Rev. Neurosci. 8, 700–711.
Friedman, N., Ito, S., Brinkman, B., Shimono, M., DeVille, R., Dahmen, K., Beggs, J., Butler, T.C., 2012. Universal critical dynamics in high resolution neuronal avalanche data. Phys. Rev. Lett. 108, 208102.
Graimann, B., Pfurtscheller, G., 2006. Quantification and visualization of event-related changes in oscillatory brain activity in the time–frequency domain. Prog. Brain Res. 159, 79–97.
Haufe, S., Nikulin, V.V., Müller, K.-R., Nolte, G., 2013. A critical assessment of connectivity measures for EEG data: a simulation study. NeuroImage 64, 120–133.
Hohlefeld, F., Huebl, J., Huchzermeyer, C., Schneider, G.-H., Schönecker, T., Kühn, A., Curio, G., Nikulin, V., 2012. Long-range temporal correlations in the subthalamic nucleus of patients with Parkinson's disease. Eur. J. Neurosci. 36, 2812–2821.
Hyvärinen, A., Oja, E., 2000. Independent component analysis: algorithms and applications. Neural Netw. 13, 411–430.
Kuramoto, Y., 2003. Chemical Oscillations, Waves, and Turbulence. Courier Dover Publications.
Linkenkaer-Hansen, K., Nikouline, V., Palva, J., Ilmoniemi, R., 2001. Long-range temporal correlations and scaling behavior in human brain oscillations. J. Neurosci. 21, 1370–1377.

Linkenkaer-Hansen, K., Monto, S., Rytsälä, H., Suominen, K., Isometsä, E., Kähkönen, S., 2005. Breakdown of long-range temporal correlations in theta oscillations in patients with major depressive disorder. J. Neurosci. 25, 10131–10137.
Meinecke, F., Ziehe, A., Kurths, J., Müller, K.-R., 2005. Measuring phase synchronization of superimposed signals. Phys. Rev. Lett. 94, 084102.
Miller, K., Sorensen, L., Ojemann, J., den Nijs, M., 2009. Power-law scaling in the brain surface electric potential. PLoS Comput. Biol. 5, e1000609.
Montez, T., Poil, S.-S., Jones, B., Manshanden, I., Verbunt, J., van Dijk, B., Brussaard, A., van Ooyen, A., Stam, C., Scheltens, P., et al., 2009. Altered temporal correlations in parietal alpha and prefrontal theta oscillations in early-stage Alzheimer disease. Proc. Natl. Acad. Sci. 106, 1614–1619.
Monto, S., Vanhatalo, S., Holmes, M., Palva, J.M., 2007. Epileptogenic neocortical networks are revealed by abnormal temporal dynamics in seizure-free subdural EEG. Cereb. Cortex 17, 1386–1393.
Moulines, E., Roueff, F., Taqqu, M.S., 2007. On the spectral density of the wavelet coefficients of long-memory time series with application to the log-regression estimation of the memory parameter. J. Time Ser. Anal. 28, 155–187.
Nikulin, V.V., Brismar, T., 2004. Long-range temporal correlations in alpha and beta oscillations: effect of arousal level and test–retest reliability. Clin. Neurophysiol. 115, 1896–1908.
Nikulin, V., Brismar, T., 2005. Long-range temporal correlations in electroencephalographic oscillations: relation to topography, frequency band, age and gender. Neuroscience 130, 549–558.
Nikulin, V.V., Nolte, G., Curio, G., 2011. A novel method for reliable and fast extraction of neuronal EEG/MEG oscillations on the basis of spatio-spectral decomposition. NeuroImage 55, 1528–1535.
Nikulin, V., Jönsson, E., Brismar, T., 2012. Attenuation of long-range temporal correlations in the amplitude dynamics of alpha and beta neuronal oscillations in patients with schizophrenia. NeuroImage 61, 162–169.
Nolte, G., Dassios, G., 2005. Analytic expansion of the EEG lead field for realistic volume conductors. Phys. Med. Biol. 50, 3807.
Nolte, G., Bai, O., Wheaton, L., Mari, Z., Vorbach, S., Hallett, M., 2004. Identifying true brain interaction from EEG data using the imaginary part of coherency. Clin. Neurophysiol. 115, 2292–2307.
Nolte, G., Ziehe, A., Nikulin, V., Schlögl, A., Krämer, N., Brismar, T., Müller, K.-R., 2008. Robustly estimating the flow direction of information in complex physical systems. Phys. Rev. Lett. 100, 234101.
Novikov, E., Novikov, A., Shannahoff-Khalsa, D., Schwartz, B., Wright, J., 1997. Scale-similar activity in the brain. Phys. Rev. E. 56, 2387.
Nunez, P., Srinivasan, R., Westdorp, A., Wijesinghe, R., Tucker, D., Silberstein, R., Cadusch, P., 1997. EEG coherency: I: statistics, reference electrode, volume conduction, laplacians, cortical imaging, and interpretation at multiple scales. Electroencephalogr. Clin. Neurophysiol. 103, 499–515.
Palva, S., Palva, J.M., 2007. New vistas for α-frequency band oscillations. Trends Neurosci. 30, 150–158.
Palva, J., Zhigalov, A., Hirvonen, J., Korhonen, O., Linkenkaer-Hansen, K., Palva, S., 2013. Neuronal long-range temporal correlations and avalanche dynamics are correlated with behavioral scaling laws. Proc. Natl. Acad. Sci. 110, 3585–3590.
Peng, C.K., Buldyrev, S.V., Havlin, S., Simons, M., Stanley, H.E., Goldberger, A.L., 1994. Mosaic organization of DNA nucleotides. Phys. Rev. E. 49, 1685–1689.
Poil, S.-S., Hardstone, R., Mansvelder, H., Linkenkaer-Hansen, K., 2012. Critical-state dynamics of avalanches and oscillations jointly emerge from balanced excitation/inhibition in neuronal networks. J. Neurosci. 32, 9817–9823.
Pritchard, W., 1992. The brain in fractal time: 1/f-like power spectrum scaling of the human electroencephalogram. Int. J. Neurosci. 66, 119–129.
Shew, W.L., Yang, H., Petermann, T., Roy, R., Plenz, D., 2009. Neuronal avalanches imply maximum dynamic range in cortical networks at criticality. J. Neurosci. 29, 15595–15600.
Shew, W.L., Yang, H., Yu, S., Roy, R., Plenz, D., 2011. Information capacity and transmission are maximized in balanced cortical networks with neuronal avalanches. J. Neurosci. 31, 55–63.
Simonsen, I., Hansen, A., Nes, O.M., 1998. Determination of the Hurst exponent by use of wavelet transforms. Phys. Rev. E. 58, 2779.
Smit, D., De Geus, E., van de Nieuwenhuijzen, M., van Beijsterveldt, C., van Baal, G., Mansvelder, H., Boomsma, D., Linkenkaer-Hansen, K., 2011. Scale-free modulation of resting-state neuronal oscillations reflects prolonged brain maturation in humans. J. Neurosci. 31, 13128–13136.
Srinivasan, R., Nunez, P., Tucker, D., Silberstein, R., Cadusch, P., 1996. Spatial sampling and filtering of EEG with spline laplacians to estimate cortical potentials. Brain Topogr. 8, 355–366.
Touboul, J., Destexhe, A., 2010. Can power-law scaling and neuronal avalanches arise from stochastic dynamics? PLoS One 5, e8982.
van den Broek, S.P., Reinders, F., Donderwinkel, M., Peters, M.J., 1998. Volume conduction effects in EEG and MEG. Electroencephalogr. Clin. Neurophysiol. 106, 522–534.
Watters, P., Martin, F., 2004. A method for estimating long-range power law correlations from the electroencephalogram. Biol. Psychol. 66, 79–89.
Ziehe, A., Müller, K.-R., 1998. TDSEP — an efficient algorithm for blind separation using time structure. Proc. Int. Conf. on Artificial Neural Networks (ICANN), pp. 675–680.
Ziehe, A., Laskov, P., Nolte, G., Müller, K.-R., 2004. A fast algorithm for joint diagonalization with non-orthogonal transformations and its application to blind source separation. J. Mach. Learn. Res. 5, 777–800.